

Direct Detection of Leptophilic Dark Matter in a Model with Radiative Neutrino Masses

Daniel Schmidt^{1,*}, Thomas Schwetz^{1,†} and Takashi Toma^{1,2,‡}

¹*Max-Planck-Institut für Kernphysik, Saupfercheckweg 1, 69117 Heidelberg, Germany*

²*Institute for Theoretical Physics, Kanazawa University, Kanazawa 920-1192, Japan*

Abstract

We consider an electro-weak scale model for Dark Matter (DM) and radiative neutrino mass generation. Despite the leptophilic nature of DM with no direct couplings to quarks and gluons, scattering with nuclei is induced at the 1-loop level through photon exchange. Effectively, there are charge-charge, dipole-charge and dipole-dipole interactions. We investigate the parameter space consistent with constraints from neutrino masses and mixing, charged lepton-flavour violation, perturbativity, and the thermal production of the correct DM abundance, and calculate the expected event rate in DM direct detection experiments. We show that current data from XENON100 start to constrain certain regions of the allowed parameter space, whereas future data from XENON1T has the potential to significantly probe the model.

*daniel.schmidt@mpi-hd.mpg.de

†schwetz@mpi-hd.mpg.de

‡t-toma@hep.s.kanazawa-u.ac.jp

1 Introduction

The Standard Model (SM) is very successful in describing the fundamental particles of our world. The only solid evidence for its failure so far is the fact that neutrinos have mass, which is a necessity due to the observation of neutrino oscillations [1–4]. Furthermore, the standard cosmological model, the Λ CDM model, provides an excellent description of our Universe, with the exception that within the SM there is no viable candidate for a Dark Matter (DM) particle, which is an important ingredient of the Λ CDM model, supported by observations such as the rotation curves of spiral galaxies [5], WMAP CMB measurements [6] and gravitational lensing [7]. Hence, both neutrinos, as well as DM require an extension of the SM. Often these two phenomena are considered separately, since they might be manifestations of physics from vastly different energy scales. Here we adopt the hypothesis that neutrino mass and DM are related, and both emerge from physics at the TeV scale. In this respect models which generate neutrino masses radiatively [8–14] are intriguing. Loop suppression factors and several powers of Yukawa couplings can bring the scale of neutrino mass generation down to the TeV, and symmetries required to stabilize DM may play a role for neutrinos, for example forbid tree-level mass terms. Recent works in this context can be found in refs. [15–32].

The so-called WIMP hypothesis suggests that DM interacts sufficiently with SM particles in order to generate the relevant abundance due to thermal freeze-out from the primordial plasma. This motivates the direct search for DM in our galaxy by looking for the scattering of DM particles with nuclei in underground detectors. Several direct detection experiments are pursuing such searches, for example the CDMS II [33], XENON100 [34, 35], CoGeNT [36], DAMA/LIBRA [37], CRESST-II [38], ZEPLIN-III [39] and KIMS [40, 41] experiments. In typical WIMP models DM interacts directly with quarks, providing DM–nucleus scattering at tree-level [42, 43]. Here we are interested in so-called “leptophilic” models, where DM couples directly only to leptons, see e.g. [44]. Even in that case, DM–nucleus interactions can be induced at loop-level due to the exchange of the photon [45]. The resulting effective interactions have been investigated in refs. [45, 46]. In the following we will consider a model where the corresponding loop-diagrams induce a magnetic and/or electric dipole moment interaction [?, 47–53].

We consider a model proposed by Ma [10], in which neutrino masses are generated through 1-loop interactions and the particles which propagate in the loop can be DM candidates, being leptophilic by construction. The DM phenomenology of the model and extended versions thereof has been studied in refs. [16–20, 30, 31] and prospects for collider searches have been studied in refs. [20, 24]. We consider the situation that the lightest right handed neutrino is the DM candidate and the second lightest right handed neutrino is almost degenerated with the DM candidate. Under this situation, elastic DM–nucleus scattering is extremely suppressed and inelastic scattering induced by a lepton-loop coupled to the photon gives the dominant contribution to the event rate in direct detection experiments. We calculate the event rate in the model and compare it with

XENON100, KIMS and DAMA data. The paper is organized as follows. In Section 2, we shortly review the model from ref. [10]. We discuss the constraints from neutrino oscillation data, lepton-flavour violation and the thermal production of the DM relic abundance. In Section 3, we discuss the inelastic scattering cross section in an effective theory approach and calculate the event rate. Moreover, monochromatic photons from the decay of the excited DM state are also discussed. We summarize and conclude in Section 4. Explicit functions needed in the effective theory approach are listed in the Appendix A.

2 The Model

2.1 Neutrino masses and mixing

The model proposed by Ma in ref. [10] is a simple extension of the SM, which correlates neutrino physics and the existence of DM. The added particles to the SM are three right handed neutrinos N_i ($i = 1, 2, 3$) and one inert Higgs doublet η . In addition, a discrete \mathbb{Z}_2 symmetry is imposed: odd for the new particles and even for SM particles. The new invariant Lagrangian is

$$\mathcal{L}_N = \overline{N}_i i \not{\partial} P_R N_i + (D_\mu \eta)^\dagger (D^\mu \eta) - \frac{M_i}{2} \overline{N}_i^c P_R N_i + h_{\alpha i} \overline{\ell}_\alpha \eta^\dagger P_R N_i + \text{h.c.}, \quad (1)$$

and the scalar potential $\mathcal{V}(\phi, \eta)$ is

$$\begin{aligned} \mathcal{V}(\phi, \eta) = & m_\phi^2 \phi^\dagger \phi + m_\eta^2 \eta^\dagger \eta + \frac{\lambda_1}{2} (\phi^\dagger \phi)^2 + \frac{\lambda_2}{2} (\eta^\dagger \eta)^2 \\ & + \lambda_3 (\phi^\dagger \phi) (\eta^\dagger \eta) + \lambda_4 (\phi^\dagger \eta) (\eta^\dagger \phi) + \frac{\lambda_5}{2} (\phi^\dagger \eta)^2 + \text{h.c.}, \end{aligned} \quad (2)$$

where ϕ is the SM Higgs doublet. The vacuum expectation value (VEV) of η is assumed to be zero, so that the discrete \mathbb{Z}_2 symmetry which guarantees the stability of DM is an exact symmetry. Thus Dirac neutrino masses are not generated through the Yukawa couplings in Eq. (1). After electroweak symmetry breaking, the SM Higgs ϕ obtains the VEV $\langle \phi^0 \rangle$ and Majorana neutrino masses are generated radiatively with the effective mass

$$(m_\nu)_{\alpha\beta} \simeq \sum_{i=1}^3 \frac{2\lambda_5 h_{\alpha i} h_{\beta i} \langle \phi^0 \rangle^2}{(4\pi)^2 M_i} I\left(\frac{M_i^2}{M_\eta^2}\right), \quad (3)$$

where M_i are the masses of the right-handed neutrinos N_i , $M_\eta^2 \simeq m_\eta^2 + (\lambda_3 + \lambda_4) \langle \phi^0 \rangle^2$, and the loop function $I(x)$ is defined as

$$I(x) = \frac{x}{1-x} \left(1 + \frac{x \log x}{1-x} \right). \quad (4)$$

These relations hold for small coupling λ_5 , which is needed in order to obtain the correct neutrino masses, see below. This assumption is justified since an extra $U(1)$ symmetry appears in the limit of $\lambda_5 \rightarrow 0$.

As shown in ref. [18], the close to tri-bimaximal mixing of the Pontecorvo-Maki-Nakagawa-Sakata (PMNS) mixing matrix is achieved by adopting the following flavour structure for the Yukawa couplings $h_{\alpha i}$ (rows are labeled by $\alpha = e, \mu, \tau$ and columns by $i = 1, 2, 3$):

$$h_{\alpha i} = \begin{pmatrix} 0 & 0 & h'_3 \\ h_1 & h_2 & h_3 \\ h_1 & h_2 & -h_3 \end{pmatrix}. \quad (5)$$

This matrix implies $\theta_{23} = \pi/4$, $\theta_{13} = 0$ and $\tan \theta_{12} = \frac{1}{\sqrt{2}} h'_3 / h_3$ ¹. From the current best fit value $\sin^2 \theta_{12} = 0.312^{+0.017}_{-0.015}$ [56] follows $h'_3 / h_3 \approx 0.95^{+0.038}_{-0.033}$. At the same time this Yukawa matrix allows to satisfy severe constraints from lepton-flavour violation, see next subsection. We write the Yukawa couplings as $h_i = |h_i| e^{i\varphi_i}$ including the phases φ_i . Neutrino masses are given in terms of the model parameters as follows:

$$|(h_1^2 + h_2^2)\Lambda_1| \simeq \frac{\sqrt{\Delta m_{\text{atm}}^2}}{2}, \quad |h_3^2 \Lambda_3| \simeq \frac{\sqrt{\Delta m_{\text{sol}}^2}}{3}, \quad \text{with} \quad \Lambda_i \equiv \frac{2\lambda_5 \langle \phi^0 \rangle^2}{(4\pi)^2 M_i} I\left(\frac{M_i^2}{M_\eta^2}\right), \quad (6)$$

where $\sqrt{\Delta m_{\text{atm}}^2}$ and $\sqrt{\Delta m_{\text{sol}}^2}$ correspond to the mass eigenvalues of the neutrino mass matrix (3), and the mass difference of N_1 and N_2 is neglected. The third mass eigenvalue is zero due to the flavour structure Eq. (5). From Eq. (6) we can estimate the required sizes for the couplings h_i and λ_5 . Assuming $I(x) \sim 1$ we obtain

$$\frac{\lambda_5 h_i^2}{10^{-11}} \sim \frac{M_i}{\langle \phi^0 \rangle} \left(\frac{\sqrt{\Delta m^2}}{0.05 \text{ eV}} \right). \quad (7)$$

Since h_i cannot be too small because of the DM relic abundance, typically λ_5 has to be tiny in order to obtain correct neutrino masses.

2.2 Lepton flavour violation

Further constraints are imposed on the parameters by limits on charged lepton flavour violation. The branching ratios for lepton flavour violating processes $\ell_\alpha \rightarrow \ell_\beta \gamma$ are given as

$$\text{Br}(\ell_\alpha \rightarrow \ell_\beta \gamma) = \frac{3\alpha_{\text{em}}}{64\pi G_F^2 M_\eta^4} \left| \sum_{i=1}^3 h_{\alpha i}^* h_{\beta i} F_2\left(\frac{M_i^2}{M_\eta^2}\right) \right|^2 \text{Br}(\ell_\alpha \rightarrow \ell_\beta \nu_\alpha \bar{\nu}_\beta), \quad (8)$$

where $\alpha_{\text{em}} = e^2/(4\pi)$ is the electromagnetic fine structure constant, G_F is the Fermi constant and M_η is the mass of η^+ which we assume to be degenerate with η^0 for simplicity. The function $F_2(x)$ is given by

$$F_2(x) = \frac{1 - 6x + 3x^2 + 2x^3 - 6x^2 \log x}{6(1-x)^4}. \quad (9)$$

¹If recent indications [55–57] for a non-zero value of the mixing angle θ_{13} should be confirmed, corrections to Eq. (5) will be necessary.

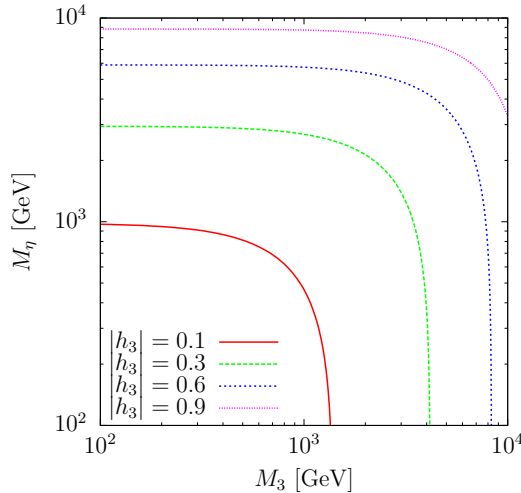


Figure 1: Contours of $\text{Br}(\mu \rightarrow e\gamma) = 2.4 \times 10^{-12}$ in the (M_3, M_η) plane for various choices of $|h_3|$. The region to the left of each contour is excluded by $\mu \rightarrow e\gamma$.

The flavour structure of Eq. (5) leads to relaxed constraints from lepton flavour violation processes such as $\mu \rightarrow e\gamma$ and $\tau \rightarrow \mu\gamma$. Because of the two zero's in (5) it follows from Eq. (8) that only the third right handed neutrino mass M_3 and the Yukawa coupling h_3 contribute to $\mu \rightarrow e\gamma$. As a result, $\tau \rightarrow \mu\gamma$ gives a more stringent constraint than $\mu \rightarrow e\gamma$ for the neutrino Yukawa couplings h_1, h_2 and the DM mass M_1 , and we can benefit from the fact that the experimental upper bound $\text{Br}(\tau \rightarrow \mu\gamma) < 4.5 \times 10^{-8}$ [58] is much looser than $\text{Br}(\mu \rightarrow e\gamma) < 2.4 \times 10^{-12}$ [59]. Contours of $\text{Br}(\mu \rightarrow e\gamma) = 2.4 \times 10^{-12}$ are shown for several $|h_3|$ values in Fig. 1. We take $M_3 = 6000$ GeV and $|h_3| = 0.3$ as a benchmark point in the following discussion. As clear from the figure, for this choice all values of M_η are allowed, and for $M_\eta \lesssim 1$ TeV we predict $\mu \rightarrow e\gamma$ close to the present bound. Eq. (7) implies then $\lambda_5 \sim 10^{-9}$.

Thanks to the restrictions of neutrino oscillation data and lepton-flavour violation there are very few independent parameters left. We can choose the following set of four independent parameters:

$$M_\eta, \quad M_1, \quad \delta \equiv M_2 - M_1, \quad \xi \equiv \text{Im}(h_2^* h_1), \quad (10)$$

with $\delta \ll M_1$. Since we fix h_3 and M_3 to the benchmark point above in order to satisfy $\mu \rightarrow e\gamma$, the relations Eq. (6) determine λ_5 as well as $|(h_1^2 + h_2^2)|$ for a given choice of M_η and M_1 . However, there is still an undetermined relative phase between h_1 and h_2 , and we define the parameter ξ , which will play an important role in the following.

2.3 DM relic abundance

We assume that the lightest right handed neutrino N_1 is the lightest of the \mathbb{Z}_2 -odd particles, and hence it will be stable and serve as the DM candidate. We assume that it

is almost degenerated with the second lightest right handed neutrino N_2 . The N_i couple to the SM only via the Yukawa interaction with the lepton doublet and therefore our DM is leptophilic². The relic density and indirect detection of DM in the model have been investigated with the flavour structure of Eq. (5) in refs. [18, 19, 22, 23]. Here we investigate the prospects for direct detection of DM in this setup for the first time.

For the thermal production of DM in this model co-annihilations between N_1 and N_2 have to be considered, since they are assumed to be highly degenerate, leading to an enhanced effective annihilation cross section [66]. The effective annihilation cross section is written as $\sigma_{\text{eff}}v = a_{\text{eff}} + b_{\text{eff}}v^2 + \mathcal{O}(v^4)$. Then the approximate analytic solution of the Boltzmann equation which describes the evolution of the DM density is given by

$$\Omega h^2 \simeq \frac{1.07 \times 10^9 x_f [\text{GeV}^{-1}]}{\sqrt{g_*} m_{\text{pl}} (a_{\text{eff}} + 3b_{\text{eff}}/x_f)}, \quad \text{with} \quad x_f = \frac{M_1}{T_f}, \quad (11)$$

where g_* is the number of relativistic degrees of freedom at the time of freeze-out T_f and $m_{\text{pl}} = 1.2 \times 10^{19}$ GeV. Taking into account co-annihilations of N_1 and N_2 we find for the coefficients a_{eff} and b_{eff} in the effective annihilation cross section

$$a_{\text{eff}} = \frac{\xi^2}{2\pi} \frac{M_1^2}{(M_\eta^2 + M_1^2)^2}, \quad (12)$$

$$b_{\text{eff}} = \frac{|h_1^2 + h_2^2|^2}{24\pi} \frac{M_1^2 (M_\eta^4 + M_1^4)}{(M_\eta^2 + M_1^2)^4} + \frac{\xi^2}{2\pi} \frac{M_1^2 (M_\eta^4 - 3M_\eta^2 M_1^2 - M_1^4)}{(M_\eta^2 + M_1^2)^4}, \quad (13)$$

where the effect of the mass difference between N_1 and N_2 is assumed to be negligible. The terms proportional to ξ^2 come from the co-annihilation process $N_1 N_2 \rightarrow \ell_\alpha \bar{\ell}_\beta$, whereas the $N_1 N_1$ and $N_2 N_2$ annihilations lead to the terms proportional to h_1^2 and h_2^2 , respectively. We observe from Eq. (12) and (13) that the s -wave (a_{eff} -term) is only present due to co-annihilations. If there is no phase difference between h_1 and h_2 , the combination of the neutrino Yukawa couplings ξ vanishes and only p -wave annihilation remains. Thus co-annihilations and a non-zero phase difference play an important role in obtaining the correct DM relic density.

For the following results we use the micrOMEGAs package [43] to calculate numerically the relic abundance of DM. In addition to $N_1 - N_2$ co-annihilations, also co-annihilations with η are important, if M_η becomes close to M_1 . The allowed parameter region in the plane of DM mass and the Yukawa coupling ξ , which is consistent with neutrino masses and mixings, lepton flavour violation, and DM relic density is shown in Fig. 2. The allowed region is colored and divided into four regions A, B, C, D, corresponding to different assumptions on the ratio M_1/M_η . The upper bound on ξ is imposed by requiring

²Another motivation for leptophilic DM may come from cosmic ray observations from the PAMELA [60] and Fermi-LAT [61, 62] experiments, finding an excess of positrons but anti-protons in agreement with expectations. In order to obtain the required count rates, however, the annihilation cross section must be boosted by a mechanism such as Sommerfeld [63] or Breit-Wigner enhancement [64, 65], beyond the model considered here.

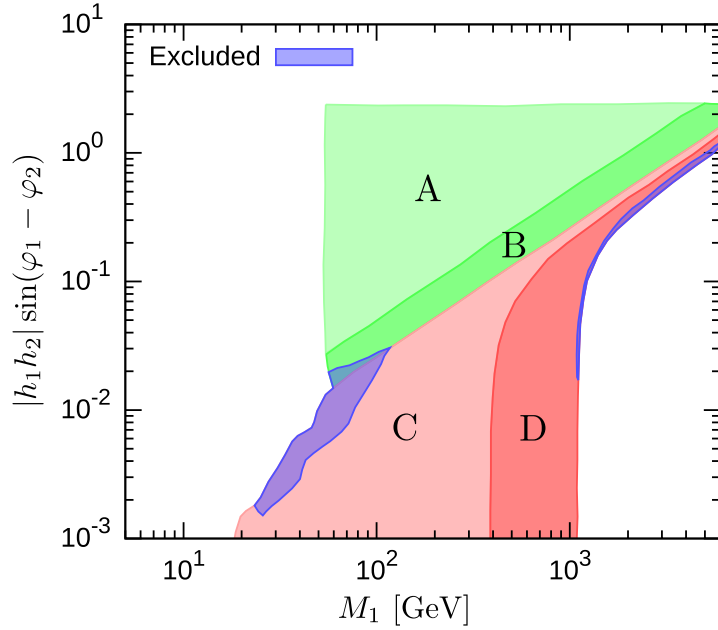


Figure 2: Region in the space of DM mass M_1 and $|h_1 h_2| \sin(\varphi_1 - \varphi_2) = \xi$ consistent with neutrino masses and mixing, lepton flavour violation, perturbativity, and the relic density of DM. The regions with different color shadings denoted by A, B, C, D, correspond to different assumptions on M_η , with A: $2.0 < M_\eta/M_1 < 20.0$, B: $1.2 < M_\eta/M_1 < 2.0$, C: $1.05 < M_\eta/M_1 < 1.20$, D: $1.0 < M_\eta/M_1 < 1.05$. The two dark (blue) regions are excluded by direct detection data from XENON100 if $\delta \ll 40$ keV (the region for $M_1 \lesssim 100$ GeV), and if $\delta \lesssim 120$ keV (the region for $M_1 \gtrsim 1$ TeV), see section 3.

perturbativity of the Yukawa couplings. The lower bound on M_1 in regions A and B is determined by the limit on $\tau \rightarrow \mu\gamma$ together with the relic abundance requirement. There is no allowed parameter region if $M_\eta/M_1 \gtrsim 20$ because taking into account perturbativity as well as $\tau \rightarrow \mu\gamma$ the annihilation cross section is suppressed by M_η^4 . If M_η/M_1 comes close to 20 we are driven to the left-upper corner of the allowed region in Fig. 2. In the parameter region C and D we have $M_\eta/M_1 < 1.2$ and co-annihilations with η become important. Without co-annihilations with η , the parameter space C and D would not appear, and we would obtain a lower bound on $|\xi|$. However, if $N_1 - \eta$ co-annihilations are relevant the correct relic density can be obtained even for vanishing ξ . In all cases we can conclude that the correct relic density is always obtained thanks to co-annihilations with either N_2 or η .

If $M_\eta \approx M_1$ one may worry about a long-lived charged particle contained in the doublet $\eta = (\eta^+, \eta^0)$. For instance, the predictions for Big Bang Nucleosynthesis (BBN) may be altered by the energy injection due to the decay of η^+ into charged leptons [67]. We have checked that for the parameter ranges of interest η decays much faster than 0.01 s unless it is degenerate with N_1 at the level of 10^{-10} , and hence BBN will be not affected.

3 Direct Detection of Leptophilic DM

3.1 Inelastic Scattering Cross Section

Inelastic scattering occurs through the effective interactions with quarks which come from the 1-loop diagrams shown in Fig. 3. The 3-point vertex effective interactions of N_1 , N_2 and γ which give a dominant contribution to the inelastic scattering are written as

$$\mathcal{L}_{\text{eff}} = ia_{12}\overline{N_2}\gamma^\mu N_1\partial^\nu F_{\mu\nu} + i\left(\frac{\mu_{12}}{2}\right)\overline{N_2}\sigma^{\mu\nu}N_1F_{\mu\nu} + ic_{12}\overline{N_2}\gamma^\mu N_1A_\mu, \quad (14)$$

where the factor i is a conventional factor to obtain real couplings a_{12} , c_{12} and μ_{12} , and $F_{\mu\nu}$ is the electromagnetic field strength. The coefficient μ_{12} is known as the transition magnetic moment between N_1 and N_2 . Elastic scattering does not occur through the effective interactions because the operators $\overline{N_1}\gamma^\mu N_1$ and $\overline{N_1}\sigma^{\mu\nu}N_1$ are identical zero for Majorana fermions. General inelastic scattering of DM has been discussed in refs. [68, 69], and inelastic scattering due to the magnetic moment interactions in ref. [50]. Loop induced DM–nucleus scattering for leptophilic DM has been pointed out in ref. [45], and the model considered here is a specific realization of “flavoured” DM discussed in ref. [46], where similar diagrams to the ones from Fig. 3 have been considered. For another recent model for magnetic inelastic DM see ref. [70].

In the model considered here, the coefficients a_{12} , c_{12} and μ_{12} are calculated as

$$a_{12} = -\sum_{\alpha} \frac{\text{Im}(h_{\alpha 2}^* h_{\alpha 1})}{2(4\pi)^2 M_\eta^2} I_a\left(\frac{M_1^2}{M_\eta^2}, \frac{m_\alpha^2}{M_\eta^2}\right), \quad (15)$$

$$\mu_{12} = -\sum_{\alpha} \frac{\text{Im}(h_{\alpha 2}^* h_{\alpha 1})}{2(4\pi)^2 M_\eta^2} 2M_1 I_m\left(\frac{M_1^2}{M_\eta^2}, \frac{m_\alpha^2}{M_\eta^2}\right), \quad (16)$$

$$c_{12} = \sum_{\alpha} \frac{\text{Im}(h_{\alpha 2}^* h_{\alpha 1})}{2(4\pi)^2 M_\eta^2} q^2 I_c\left(\frac{M_1^2}{M_\eta^2}, \frac{m_\alpha^2}{M_\eta^2}\right), \quad (17)$$

where q^2 is the momentum transfer and the explicit forms of the function $I_a(x, y)$, $I_m(x, y)$ and $I_c(x, y)$, which come from the loop integrals, are given in Appendix A. Eq. (5) implies that $\text{Im}(h_{\alpha 2}^* h_{\alpha 1}) = \xi$ and therefore the parameter ξ responsible for $N_1 - N_2$ co-annihilations controls also the effective interactions of DM with nuclei.

From the effective interactions, we can obtain three types of differential scattering cross sections with a nucleus which has atomic number Z , mass number A , mass m_A , spin J_A and magnetic moment μ_A , see e.g., [46, 50]:

$$\frac{d\sigma_{CC}}{dE_R} = \frac{Z^2 b_{12}^2 m_A}{2\pi v^2} F^2(E_R), \quad (18)$$

$$\frac{d\sigma_{DC}}{dE_R} = \frac{Z^2 \alpha_{\text{em}} \mu_{12}^2}{E_R} \left[1 - \frac{E_R}{v^2} \left(\frac{1}{2m_A} + \frac{1}{M_1} \right) - \frac{\delta}{v^2} \frac{1}{\mu_{\text{DM}}} - \frac{\delta^2}{v^2} \frac{1}{2m_A E_R} \right] F^2(E_R), \quad (19)$$

$$\frac{d\sigma_{DD}}{dE_R} = \frac{\mu_A^2 \mu_{12}^2 m_A}{\pi v^2} \left(\frac{J_A + 1}{3J_A} \right) F_D^2(E_R), \quad (20)$$

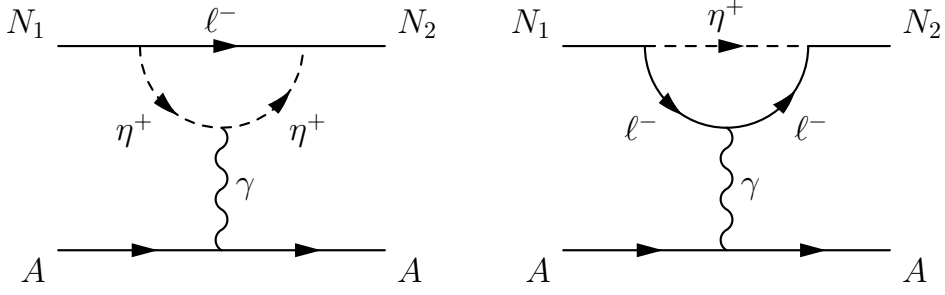


Figure 3: Diagrams for the inelastic scattering process of N_1 off a nucleus A .

with the coefficient

$$b_{12} = (a_{12} + c_{12}/q^2)e. \quad (21)$$

The cross sections Eq. (18), (19) and (20) are called charge-charge (CC), dipole-charge (DC), and dipole-dipole (DD) coupling, respectively. Here E_R is the recoil energy, the parameter δ is the mass difference between N_2 and N_1 i.e., $\delta = M_2 - M_1$ and μ_{DM} is the DM-nucleus reduced mass. Magnetic moments of several nuclei are shown in Tab. 1. $F(E_R)$ is the nuclear form factor for which we use the parametrization

$$F(E_R) = \frac{3 [\sin(\kappa r) - \kappa r \cos(\kappa r)]}{(\kappa r)^3} e^{-\kappa^2 s^2/2}, \quad (22)$$

with $\kappa = \sqrt{2m_A E_R}$, $r = \sqrt{R^2 - 5s^2}$, $R \simeq 1.2A^{1/3}$ fm and $s \simeq 1$ fm. $F_D(E_R)$ is the nuclear magnetic form factor and it is not well-known, see e.g., the discussion in ref. [50]. We adopt the following approximation for $F_D(E_R)$. The magnetic moment of a nucleus receives contributions from the spin $\langle S_{n,p} \rangle$ as well as orbital momentum $\langle L_{n,p} \rangle$ of the neutrons and protons:

$$\mu_A = g_p^s \langle S_p \rangle + g_n^s \langle S_n \rangle + g_p^l \langle L_p \rangle + g_n^l \langle L_n \rangle. \quad (23)$$

We approximate the magnetic form factor by neglecting the orbital momentum contribution³ and use the spin form factors weighted by the corresponding g^s factors:

$$F_D(E_R) \approx \frac{g_p^s S_p(q^2) + g_n^s S_n(q^2)}{g_p^s S_p(0) + g_n^s S_n(0)}. \quad (24)$$

The spin-dependent form factors and $g_{p,n}^s$ factors are taken from refs. [71, 72].

In addition to the CC, DC, DD interactions from Eqs. (18), (19), (20) also a charge-dipole coupling exists. However there is an additional suppression factor of q^2 compared

³The ratio of spin and orbital contributions to the magnetic moment in Eq. (23) are 0.59 : 0.41 for Sodium, 0.52 : 0.48 for Iodine, 0.96 : 0.04 for Xenon, -0.38 : 1.38 for Cesium. Therefore, neglecting the orbital contribution is an excellent approximation for Xenon. For the other nuclei this introduces an error of about a factor 2 and therefore the limits derived from KIMS and DAMA should be considered only approximate.

	$^{19}_9\text{F}$	$^{23}_{11}\text{Na}$	$^{73}_{32}\text{Ge}$	$^{127}_{53}\text{I}$	$^{131}_{54}\text{Xe}$	$^{133}_{55}\text{Cs}$	$^{183}_{74}\text{W}$
J_A	1/2	3/2	9/2	5/2	3/2	7/2	1/2
μ_A/μ_N	2.629	2.218	-0.879	2.813	0.692	2.582	0.118

Table 1: Magnetic moments for several nuclei in units of μ_N where $\mu_N = e/2m_p$ is the nuclear magneton [73].

to the other couplings, thus it can be neglected. The DC coupling is singular at $E_R = 0$. Therefore the predicted event rate of the DC coupling is enhanced at low recoil energies due to the singularity, and we cannot define a total cross section at the zero momentum transfer limit σ_{DC}^0 . This situation is the same as in Coulomb scattering.

3.2 Comparison of the Predicted Event Rate with Experiments

We compare the event rate calculated from the effective interactions with XENON100 [35], KIMS [41] and DAMA [37] data. The DD coupling might be important for KIMS or DAMA [50] since in these experiments, the target nuclei are iodine (I) and cesium (Cs) for KIMS, iodine and sodium (Na) for DAMA, which have a large nuclear magnetic moment as can be seen from Tab. 1. The event rate is written as

$$\frac{dR}{dE_R} = \sum_{\text{nuclei}} \frac{\rho_\odot}{M_1} \frac{1}{M_{\text{det}}} \int_{v>v_{\min}} \frac{d\sigma}{dE_R} v f(\mathbf{v}) d^3v, \quad (25)$$

where $\rho_\odot \simeq 0.3 \text{ GeVcm}^{-3}$ is the local DM density, M_{det} is the mass of target material, v_{\min} is the minimum velocity required for DM to scatter off a nucleus with recoil energy E_R ,

$$v_{\min} = \frac{1}{\sqrt{2m_A E_R}} \left(\frac{m_A E_R}{\mu_{\text{DM}}} + \delta \right), \quad (26)$$

and $f(\mathbf{v})$ is the local DM velocity distribution function in the rest frame of the Earth. It is obtained by a Galilean transformation from a Maxwell-Boltzmann distribution in the rest frame of the galaxy with the velocity dispersion $v_0 = 220 \text{ km/s}$ and the escape velocity from the galaxy $v_{\text{esc}} = 544 \text{ km/s}$. The velocity distribution function $f(\mathbf{v})$ is normalized to $\int f(\mathbf{v}) d^3v = 1$. The relative velocity of the Earth to the galaxy is $v_e = v_\odot + v_{\text{orb}} \cos \gamma \cos [2\pi(t - t_0)/\text{year}]$ with $v_\odot = v_0 + 12 \text{ km/s}$, $v_{\text{orb}} = 30 \text{ km/s}$, $\cos \gamma = 0.51$ and $t_0 = \text{June 2nd}$. We must evaluate the following velocity integrals to predict the event rate:

$$\zeta_1(v_{\min}, v_e) = \int_{v_{\min}}^{\infty} \frac{f(\mathbf{v} + \mathbf{v}_e)}{v} d^3v, \quad (27)$$

$$\zeta_2(v_{\min}, v_e) = \int_{v_{\min}}^{\infty} v f(\mathbf{v} + \mathbf{v}_e) d^3v. \quad (28)$$

The analytic formulas for the DM velocity integrals given in refs. [53, 74] are used. The total predicted event rate in the XENON100, DAMA, and KIMS experiments is obtained

	Energy range	Quenching factor
XENON100	8.4 – 44.6 keV	—
KIMS	3.6 – 5.8 keVee	0.1 (Cs), 0.1 (I)
DAMA	2 – 8 keVee	0.3 (Na), 0.09 (I)

Table 2: The energy range and the quenching factor for the experiments XENON100 [35], KIMS [41], and DAMA [37]. For XENON100 we use the same light-yield function L_{eff} as in ref. [35].

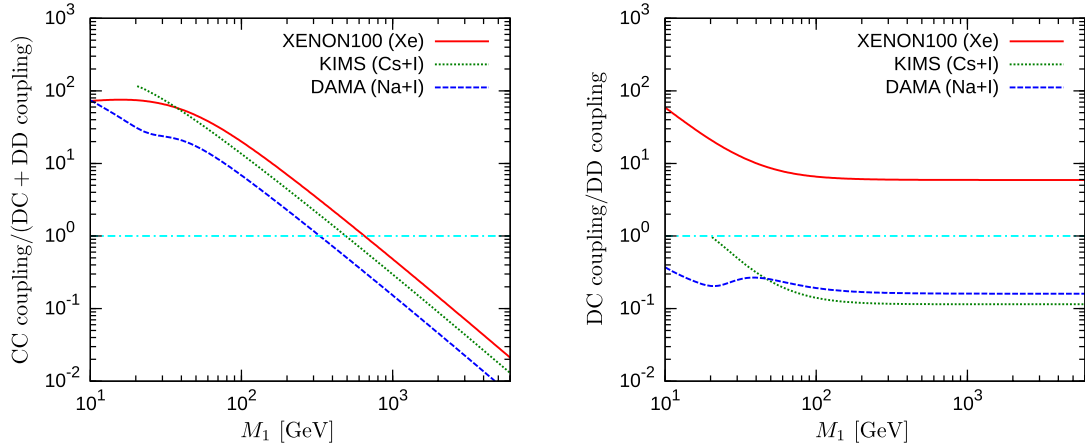


Figure 4: Relative contributions of the charge-charge (CC), dipole-charge (DC), and dipole-dipole (DD) interactions to the total predicted event rate in XENON100, KIMS, and DAMA. The left panel shows the contribution from CC relative to the sum of DC and DD, the right panel shows the ratio of the DC and DD contributions. We assume $M_\eta/M_1 = 1.5$ and $\delta = 0$.

by integrating the differential event rate with respect to an appropriate recoil energy range. We use the energy range and the quenching factors shown in Tab. 2. The quenching factor is the ratio of the energy deposited in scintillation light to the total nuclear recoil energy.

In Fig. 4 we illustrate the relative importance of the the CC, DC, DD interactions from Eqs. (18), (19), (20) for the XENON100, KIMS, and DAMA experiments by calculating the total event rate induced from each of the three interaction types separately. We observe from the left panel that typically CC interactions are more important for small masses M_1 , which follows from the different dependence on the DM mass of b_{12} and μ_{12} . The value M_1 where CC becomes subdominant depends on the ratio M_η/M_1 . The right panel of Fig. 4 shows that for XENON100 the DC coupling is more important, whereas for KIMS and DAMA DD dominates, because of the large magnetic moments of iodine and sodium. The features of the DAMA curves around $M_1 \simeq 20$ GeV in both panels are a consequence of the presence of the two elements (I and Na) with rather different masses. In general the relative importance of CC, DC, DD depends on the ratio M_η/M_1 and to a lesser extent on δ . The main conclusion is that depending on the region in the parameter

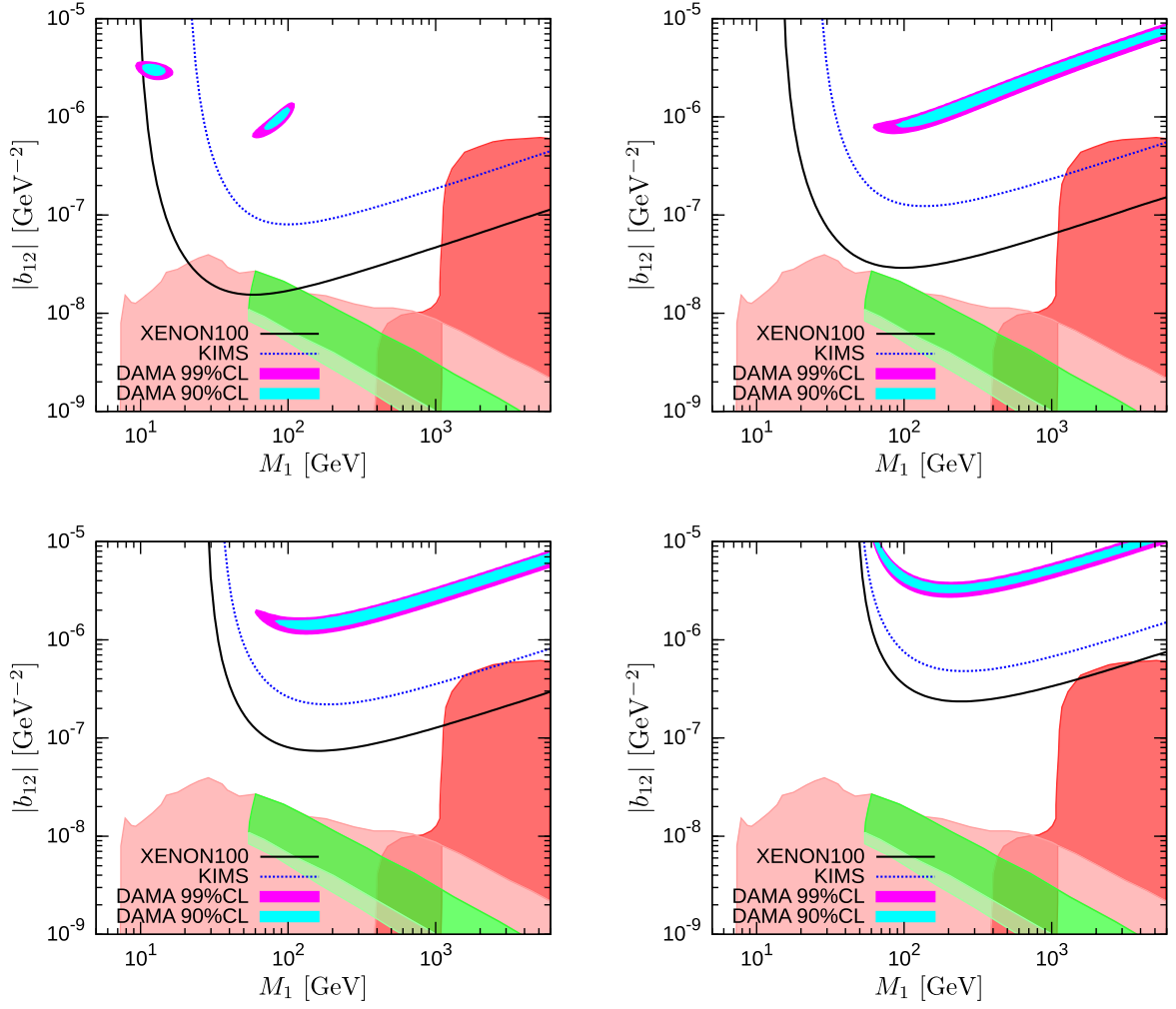


Figure 5: Bounds from XENON100, KIMS and allowed regions for DAMA in the $(M_1, |b_{12}|)$ plane (charge-charge interaction). The mass difference δ is taken as 0 keV (the left top panel), 40 keV (the right top panel), 80 keV (the left bottom panel) and 120 keV (the right bottom panel). The shaded regions correspond to the values of b_{12} predicted in the allowed parameter space of the model, as shown in Fig. 2, with the same color shading for different values of the ratio M_η/M_1 .

space and depending on the considered experiment, any of the three interaction types can be important and all of them have to be taken into account.

In order to derive constraints on the model we calculate the total event rate for XENON100 and KIMS in the energy range given in Tab. 2 and require that the predicted rate is less than $0.0017, 0.0098 \text{ kg}^{-1}\text{day}^{-1}$ for XENON100 and KIMS, respectively. The upper bounds are obtained from the observed 3 events with 3σ of the statistical error in the 48 kg fiducial volume during 100.9 live days exposure in the signal region for XENON100 [35], and from ref. [41] for KIMS. For DAMA we perform a χ^2 fit to the modulation amplitude in bins of observed scintillation energy between 2 and 8 keVee.

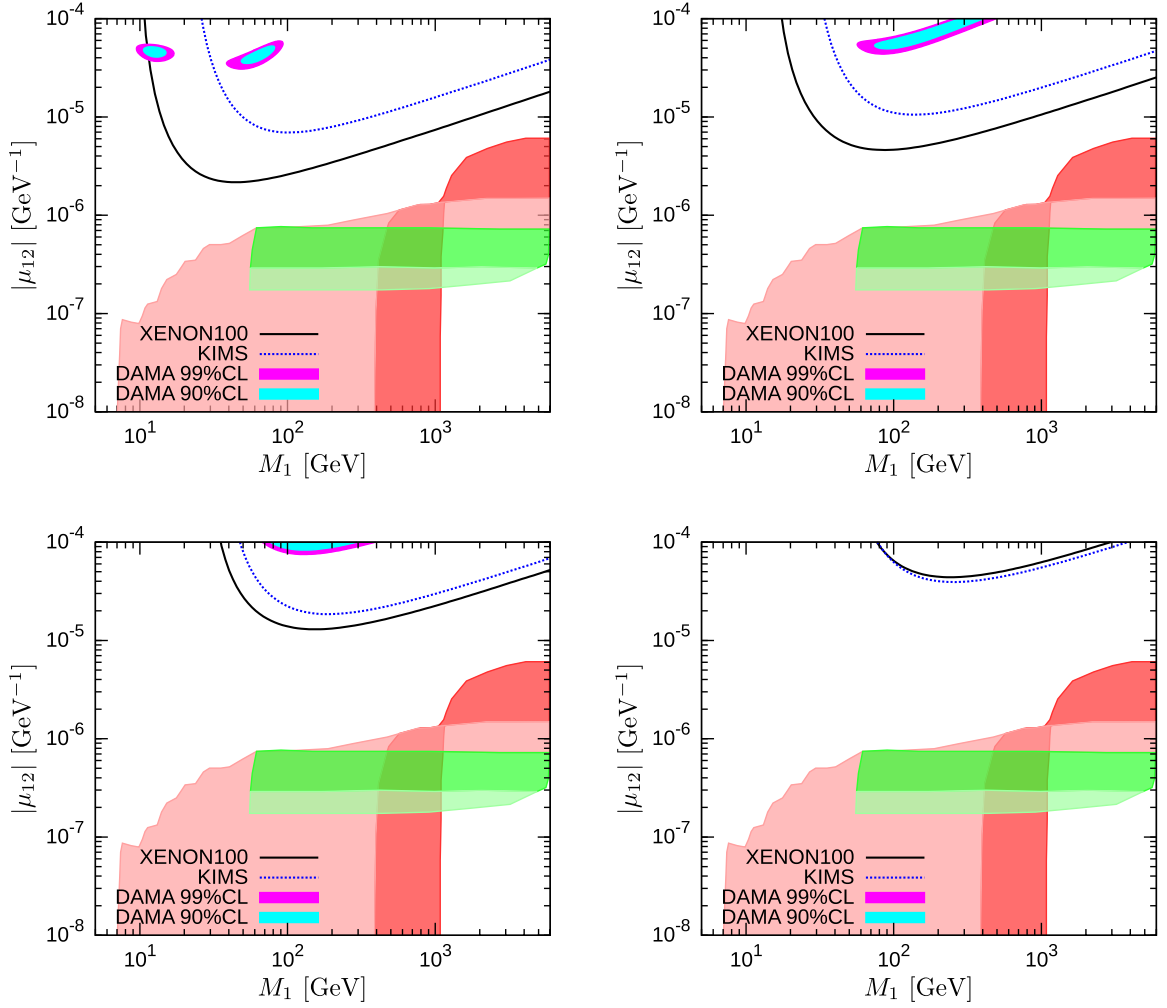


Figure 6: Bounds from XENON100, KIMS and allowed regions for DAMA in the $(M_1, |\mu_{12}|)$ plane (dipole-charge and dipole-dipole interaction). The mass difference δ is taken as 0 keV (the left top panel), 40 keV (the right top panel), 80 keV (the left bottom panel) and 120 keV (the right bottom panel). The shaded regions correspond to the values of μ_{12} predicted in the allowed parameter space of the model, as shown in Fig. 2, with the same color shading for different values of the ratio M_η/M_1 .

In Fig. 5 and Fig. 6 we show the bounds from XENON100, KIMS and allowed regions from DAMA for the coefficients b_{12} (see Eq. (18)) and μ_{12} (see Eqs. (19, 20)), respectively. These bounds are compared to the regions as predicted in the model according to Eqs. (15, 17, 21) for b_{12} and Eq. (16) for μ_{12} . The colored regions correspond to the regions shown in Fig. 2, satisfying constraints from neutrino masses and mixing, charged lepton-flavour violation, the relic DM density, and perturbativity. The ratio M_η/M_1 is taken in the range $1 \leq M_\eta/M_1 \leq 20$, with the same color shading as in Fig. 2. There is no allowed parameter space for $M_\eta/M_1 \gtrsim 20$, as discussed earlier.

We observe that the values of $|b_{12}|$ and $|\mu_{12}|$ obtained in this model are too small to

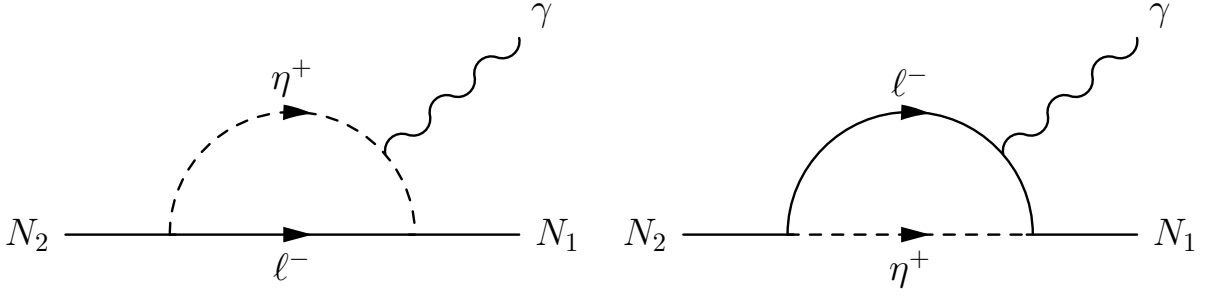


Figure 7: Decay process of N_2 .

account for the signal in DAMA. For very small mass splittings δ between N_1 and N_2 some regions of the parameter space are excluded by XENON100 data. The constraints become weaker for larger δ , since increasing inelasticity suppresses the scattering event rate. The two regions excluded by the XENON100 curve in the top-left panel in Fig. 5 (where $\delta = 0$) correspond to the two dark-blue regions in Fig. 2. The excluded region around $M_1 \simeq 100$ GeV becomes allowed for $\delta \gtrsim 40$ GeV (see top-right panel). Relatively large values of $|b_{12}|$ are obtained for close to degenerate N_1 and η , $M_\eta/M_1 \lesssim 1.05$ (dark-red region), because of the behavior of the function $I_a(x, y)$ near $x = 1$, where $I_a(x, y) \sim y^{-1}$ and $y = m_\alpha^2/M_\eta^2$ is small. The region excluded by XENON100 for $M_1 \simeq M_\eta \sim 2$ TeV becomes allowed for $\delta \gtrsim 120$ keV (bottom-right panel). By comparing Figs. 5 and 6 we observe that the model predicts values of μ_{12} too small to be tested by current direct detection data. The enhancement for the transition magnetic moment $|\mu_{12}|$ for $M_\eta/M_1 \lesssim 1.05$ is less than for $|b_{12}|$ due to a different behavior of the loop functions $I_a(x, y)$ and $I_m(x, y)$.

We conclude that current data from XENON100 starts to exclude some parameter space of the model, mainly in case of degenerate configurations $M_1 \simeq M_2$ or $M_1 \simeq M_2 \simeq M_\eta$. Future data from the XENON1T experiment will dig deeply into the allowed parameter region of the model. We note however, that no signal is guaranteed for direct detection. In the $N_1 - \eta$ co-annihilation region (dark- and light-red regions, where $M_\eta/M_1 < 1.2$) no lower bound on the parameter $|\xi|$ is obtained (compare Fig. 2), leading to arbitrarily small values of $|b_{12}|$ and $|\mu_{12}|$, which implies a vanishing signal in direct detection experiments.

3.3 Monochromatic Photon from the Decay of N_2

The excited DM state N_2 decays to N_1 and a photon through the transition magnetic moment. The diagrams of the decay process are shown in Fig. 7 and the decay width is calculated as

$$\Gamma(N_2 \rightarrow N_1 \gamma) = \frac{\mu_{12}^2}{\pi} \delta^3. \quad (29)$$

Notice that the effective interaction b_{12} does not contribute to the decay width since the emitted photon is on-shell. The decay of N_2 produces a monochromatic photon of energy

$E_\gamma \simeq \delta$. If the decay happens inside a DM detector this monochromatic photon would contribute to the electromagnetic event rate. Although typically such events are rejected in order to search for nuclear recoils one may be able to place constraints on the model by requiring that the electromagnetic event rate induced by the decay of N_2 has to be less than the observed rate. A similar mechanism has been used in Ref. [75] in order to explain the DAMA modulation signal.

Following Ref. [75] we estimate the photon induced event rate in the model under consideration for the XENON100 experiment. The excited state N_2 is produced by the inelastic scattering with nuclei inside the Earth which is composed of various elements such as Fe, O and Si. The event rate in XENON100 is given by

$$\frac{dR_\gamma}{dE_R} = \frac{\rho_\odot}{M_1 \rho_{\text{Xe}}} \sum_{i=\text{nuclei}} \int_{v>v_{\min}} d^3v \frac{d\sigma_i}{dE_R} v f(\mathbf{v}) \int_{\text{Earth}} d^3r n_i(\mathbf{r}) P(\mathbf{r}, v), \quad (30)$$

where ρ_{Xe} is the mass density of the XENON detector 21.9 g/cm^3 , σ_i is the total inelastic scattering cross section which includes the charge-charge, dipole-charge and dipole-dipole interactions, and $n_i(\mathbf{r})$ is the number density for the given nucleus i inside the Earth. Note that E_R is the nuclear recoil energy in the $N_1 + A \rightarrow N_2 + A$ scattering process. The contribution of the dipole-dipole interaction is much smaller than the ones from the charge-charge and dipole-charge interactions since the fraction of isotopes with a sizable magnetic moment in the Earth is less than a few %. In Eq. (30), $P(\mathbf{r}, v)$ is the probability that an N_2 which is produced by the scattering of DM with velocity v at the position \mathbf{r} decays inside the XENON100 detector. It is given by

$$P(\mathbf{r}, v) = \frac{1}{4\pi(\mathbf{r} - \mathbf{r}_{\text{Xe}})^2} \frac{\Gamma}{v_f} e^{-\Gamma|\mathbf{r} - \mathbf{r}_{\text{Xe}}|/v_f}, \quad (31)$$

where $v_f = \sqrt{v^2 - 2(\delta + E_R)/M_1}$ is the velocity of the produced N_2 , and \mathbf{r}_{Xe} is the position of XENON detector on the Earth. The total gamma event rate R_γ is obtained by integrating Eq. (30) over the recoil energy E_R .

In order to obtain a rough estimate of the induced event rate we introduce some approximations. We use the averaged number density of the elements in the Earth $\bar{n} \simeq 9.85 \times 10^{22} \text{ cm}^{-3}$, the averaged atomic number $\bar{Z} \simeq 29.9$ and the averaged magnetic moment of nuclei $\bar{\mu}_A/\mu_N \simeq 3.46 \times 10^{-2}$, which are calculated by taking into account the structure of the Earth such as the crust, mantle and core [75]. Replacing $n_i(\mathbf{r})$ by its average, it can be pulled out of the r -integral in Eq. (30) and the integration is performed analytically:

$$\int_{\text{Earth}} d^3r P(\mathbf{r}, v) = \frac{1}{2} \left[\frac{v_f}{2\Gamma r_\oplus} (e^{-2\Gamma r_\oplus/v_f} - 1) + 1 \right], \quad (32)$$

where $r_\oplus = 6.4 \times 10^6 \text{ m}$ is the radius of the Earth. The remaining integrations over v and E_R are done numerically.

With this approximation we estimate the total predicted event rate in XENON100 for typical parameters of the model. We find that the maximal rate is approximately

$R_{\gamma}^{\max} \simeq 2.0 \times 10^{-7} \text{ kg}^{-1} \text{ day}^{-1}$, when $\delta \simeq 40 \text{ keV}$ and $M_1/M_{\eta} = 1$. This result should be compared with 22 events obtained in the electromagnetic band in the 40 kg fiducial volume during 11.17 live days exposure in the DM search window by XENON100 [34]. Hence, since the predicted event rate is several orders of magnitude smaller we conclude that the monochromatic photon from the N_2 decay will not lead to any observable signal in DM direct detection experiments.

4 Summary and Conclusions

We have considered a model proposed by Ma [10], providing an economical extension of the Standard Model to accommodate neutrino masses and DM. The Standard Model is extended by three fermion singlets N_i (“right handed neutrinos”) and an inert scalar doublet η , where the new particles transform odd under a \mathbb{Z}_2 symmetry, making the lightest of them a stable DM candidate. In our case N_1 is the DM particle. We investigate the parameter space of the model consistent with neutrino masses and mixings, bounds on charged lepton-flavour violation, perturbativity, and the correct relic DM abundance due to the thermal freeze-out mechanism. We find that in order to obtain the correct relic DM abundance co-annihilations are always important, either between the two lightest fermion singlets N_1 and N_2 , or between N_1 and the inert doublet η .

In this model DM has no direct couplings to quarks and gluons. Despite this leptophilic nature of DM, scattering off nuclei is possible at 1-loop level by photon exchange. We have calculated the relevant loop processes in an effective field theory approach. One obtains effective charge-charge, dipole-charge, and dipole-dipole interactions between DM and nuclei, leading to a non-vanishing scattering rate in DM direct detection experiments. The scattering is inelastic and in order to obtain a sizable scattering rate N_1 and N_2 have to be highly degenerate, with mass differences δ less than few 100 keV. This is consistent with the need for co-annihilations to obtain the correct relic abundance. Although the scattering cross section in this model is too small to account for the DAMA annual modulation signal, we find that for mass differences $\delta \lesssim 120 \text{ keV}$ current data from the XENON100 experiment start to exclude certain regions of the parameter space. The predicted event rate for XENON100 is dominated by the charge-charge interaction. Future data, for example from XENON1T, will significantly dig into the allowed parameter space and provide a stringent test for the model.

Acknowledgments

T.T. is supported by Young Researcher Overseas Visits Program for Vitalizing Brain Circulation Japanese in JSPS. D.S. is supported by the International Max Planck Research School for Precision Tests of Fundamental Symmetries. T.T. would like to thank Daijiro Suematsu for useful comments and the Particle and Astroparticle Physics group at MPIK

Heidelberg. The numerical calculations were partially carried out on SR16000 at YITP in Kyoto University.

Appendix A

Explicit Functions for the Effective Interactions

Here we give the explicit functions for the effective interactions. The functions $I_a(x, y)$ and $I_m(x)$ are given as follows,

$$I_a(x, y) = \frac{1}{3} \int_0^1 \frac{3u^2 - 6u + 1}{xu^2 - (1 + x - y)u + 1} du, \quad (33)$$

$$I_m(x, y) = - \int_0^1 \frac{u(1 - u)}{xu^2 - (1 + x - y)u + 1} du. \quad (34)$$

The analytic formulas of these integrations are given as follows.

(i) If $(1 + x - y)^2 - 4x > 0$,

$$I_a(x, y) = \frac{1}{x} \left[1 + \frac{3A_+^2 - 6A_+ + 1}{3(A_+ - A_-)} \log \left| \frac{A_+ - 1}{A_+} \right| - \frac{3A_-^2 - 6A_- + 1}{3(A_+ - A_-)} \log \left| \frac{A_- - 1}{A_-} \right| \right], \quad (35)$$

$$I_m(x, y) = \frac{1}{x} \left[1 + \frac{A_+(A_+ - 1)}{A_+ - A_-} \log \left| \frac{A_+ - 1}{A_+} \right| - \frac{A_-(A_- - 1)}{A_+ - A_-} \log \left| \frac{A_- - 1}{A_-} \right| \right]. \quad (36)$$

(ii) If $(1 + x - y)^2 - 4x = 0$,

$$I_a(x, y) = \frac{1}{x} \left[1 + 2(A_0 - 1) \log \left| \frac{A_0 - 1}{A_0} \right| + \frac{3A_0^2 - 6A_0 + 1}{3A_0(A_0 - 1)} \right], \quad (37)$$

$$I_m(x, y) = \frac{1}{x} \left[2 + (2A_0 - 1) \log \left| \frac{A_0 - 1}{A_0} \right| \right]. \quad (38)$$

(iii) If $(1 + x - y)^2 - 4x < 0$,

$$I_a(x, y) = \frac{1}{x} \left[1 + \frac{B_+ + B_- - 2}{2} \log \left| \frac{(B_+ - 1)^2 + (B_- - 1)^2}{B_+^2 + B_-^2} \right| + \frac{6(B_+ - 1)(B_- - 1) - 4}{3(B_+ - B_-)} \text{Tan}^{-1} \left(\frac{B_+ - B_-}{B_+^2 + B_-^2 - B_+ - B_-} \right) \right], \quad (39)$$

$$I_m(x, y) = \frac{1}{x} \left[1 + \frac{B_+ + B_- - 1}{2} \log \left| \frac{(B_+ - 1)^2 + (B_- - 1)^2}{B_+^2 + B_-^2} \right| + \frac{(2B_+ - 1)(2B_- - 1) - 1}{2(B_+ - B_-)} \text{Tan}^{-1} \left(\frac{B_+ - B_-}{B_+^2 + B_-^2 - B_+ - B_-} \right) \right]. \quad (40)$$

A_{\pm} , A_0 and B_{\pm} are defined as

$$\begin{aligned} A_{\pm} &\equiv \frac{1+x-y \pm \sqrt{(1+x-y)^2 - 4x}}{2x}, \\ A_0 &\equiv \frac{1+x-y}{2x}, \\ B_{\pm} &\equiv \frac{1+x-y \pm \sqrt{4x - (1+x-y)^2}}{2x}. \end{aligned}$$

The function $I_c(x, y)$ is the same as $I_m(x, y)$. These functions are continuous and smooth for $0 \leq x, y \leq 1$. For $0 \simeq y \ll x \ll 1$, these functions approach to

$$I_a(x, y) \rightarrow \frac{1}{2} + \frac{2}{3} \log y, \quad (41)$$

$$I_m(x, y) \rightarrow -\frac{1}{2}. \quad (42)$$

Therefore, the obtained parameters $|b_{12}|$ and $|\mu_{12}|$ at lowest order agree with the result of ref. [46] where the parameter λ^2 in ref. [46] corresponds to $\text{Im}(h_{\alpha 2}^* h_{\alpha 1})/2$ in our notation. The difference of the relative sign comes from the definition of the effective operators.

References

- [1] Y. Fukuda *et al.* [Super-Kamiokande Collaboration], Phys. Rev. Lett. **81**, 1562 (1998) [[arXiv:hep-ex/9807003](#)].
- [2] Q. R. Ahmad *et al.* [SNO Collaboration], Phys. Rev. Lett. **89**, 011301 (2002) [[arXiv:nucl-ex/0204008](#)].
- [3] T. Araki *et al.* [KamLAND Collaboration], Phys. Rev. Lett. **94**, 081801 (2005) [[arXiv:hep-ex/0406035](#)].
- [4] P. Adamson *et al.* [MINOS Collaboration], Phys. Rev. Lett. **101**, 131802 (2008) [[arXiv:0806.2237](#) [hep-ex]].
- [5] K. G. Begeman, A. H. Broeils and R. H. Sanders, Mon. Not. Roy. Astron. Soc. **249**, 523 (1991).
- [6] E. Komatsu *et al.* [WMAP Collaboration], Astrophys. J. Suppl. **192**, 18 (2011) [[arXiv:1001.4538](#) [astro-ph.CO]].
- [7] R. Massey *et al.*, Nature **445**, 286 (2007) [[arXiv:astro-ph/0701594](#)].
- [8] A. Zee, Phys. Lett. B **93**, 389 (1980) [Erratum-ibid. B **95**, 461 (1980)].
- [9] A. Zee, Phys. Lett. B **161**, 141 (1985).
- [10] E. Ma, Phys. Rev. D **73**, 077301 (2006) [[arXiv:hep-ph/0601225](#)].
- [11] A. Zee, Nucl. Phys. B **264**, 99 (1986).

- [12] K. S. Babu, Phys. Lett. B **203**, 132 (1988).
- [13] L. M. Krauss, S. Nasri and M. Trodden, Phys. Rev. D **67**, 085002 (2003) [[arXiv:hep-ph/0210389](#)].
- [14] M. Aoki, S. Kanemura and O. Seto, Phys. Rev. Lett. **102**, 051805 (2009) [[arXiv:0807.0361](#)].
- [15] N. Sahu and U. Sarkar, Phys. Rev. D **78**, 115013 (2008) [[arXiv:0804.2072](#)].
- [16] J. Kubo, E. Ma and D. Suematsu, Phys. Lett. B **642**, 18 (2006) [[arXiv:hep-ph/0604114](#)].
- [17] Y. Kajiyama, J. Kubo and H. Okada, Phys. Rev. D **75**, 033001 (2007) [[arXiv:hep-ph/0610072](#)].
- [18] D. Suematsu, T. Toma and T. Yoshida, Phys. Rev. D **79**, 093004 (2009) [[arXiv:0903.0287](#)].
- [19] D. Suematsu, T. Toma and T. Yoshida, Phys. Rev. D **82**, 013012 (2010) [[arXiv:1002.3225](#)].
- [20] D. Aristizabal Sierra, J. Kubo, D. Restrepo, D. Suematsu and O. Zapata, Phys. Rev. D **79**, 013011 (2009) [[arXiv:0808.3340](#)].
- [21] K. S. Babu and E. Ma, Int. J. Mod. Phys. A **23**, 1813 (2008) [[arXiv:0708.3790](#)].
- [22] D. Suematsu and T. Toma, Nucl. Phys. B **847**, 567 (2011) [[arXiv:1011.2839](#)].
- [23] H. Fukuoka, D. Suematsu and T. Toma, JCAP **1107**, 001 (2011) [[arXiv:1012.4007](#)].
- [24] M. Aoki and S. Kanemura, Phys. Lett. B **689**, 28 (2010) [[arXiv:1001.0092](#)].
- [25] M. Aoki, S. Kanemura, T. Shindou and K. Yagyu, JHEP **1007**, 084 (2010) [Erratum-ibid. **1011**, 049 (2010)] [[arXiv:1005.5159](#)].
- [26] M. Lindner, D. Schmidt and T. Schwetz, [arXiv:1105.4626](#).
- [27] T. Li and W. Chao, Nucl. Phys. B **843**, 396 (2011) [[arXiv:1004.0296](#)].
- [28] S. Kanemura, T. Nabeshima and H. Sugiyama, [arXiv:1106.2480](#).
- [29] A. Ibarra and C. Simonetto, [arXiv:1107.2386](#).
- [30] Y. Kajiyama, H. Okada and T. Toma, Eur. Phys. J. C **71**, 1688 (2011) [[arXiv:1104.0367](#)].
- [31] Y. Kajiyama, H. Okada and T. Toma, [arXiv:1109.2722](#).
- [32] M. Aoki, J. Kubo, T. Okawa and H. Takano, [arXiv:1110.5403](#).
- [33] Z. Ahmed *et al.* [The CDMS-II Collaboration], Science **327**, 1619 (2010) [[arXiv:0912.3592](#) [astro-ph.CO]].
- [34] E. Aprile *et al.* [XENON100 Collaboration], Phys. Rev. Lett. **105**, 131302 (2010) [[arXiv:1005.0380](#) [astro-ph.CO]].

- [35] E. Aprile *et al.* [XENON100 Collaboration], Phys. Rev. Lett. **107** (2011) 131302 [[arXiv:1104.2549](#)].
- [36] C. E. Aalseth *et al.* [CoGeNT collaboration], Phys. Rev. Lett. **106**, 131301 (2011) [[arXiv:1002.4703](#)].
- [37] R. Bernabei *et al.*, Eur. Phys. J. C **67**, 39 (2010) [[arXiv:1002.1028](#)].
- [38] G. Angloher *et al.*, [arXiv:0809.1829](#) [astro-ph].
- [39] V. N. Lebedenko *et al.*, Phys. Rev. D **80**, 052010 (2009) [[arXiv:0812.1150](#)].
- [40] H. S. Lee *et al.* [KIMS Collaboration], Phys. Rev. Lett. **99**, 091301 (2007) [[arXiv:0704.0423](#)].
- [41] S. K. KIM, Recent results from kims, talk at TAUP 2011, “12th International Conference on Topics in Astroparticle and Underground Physics”, 2011.
- [42] G. Jungman, M. Kamionkowski and K. Griest, Phys. Rept. **267**, 195 (1996) [[hep-ph/9506380](#)].
- [43] G. Belanger, F. Boudjema, A. Pukhov and A. Semenov, Comput. Phys. Commun. **180**, 747 (2009) [[arXiv:0803.2360](#)].
- [44] P. J. Fox and E. Poppitz, Phys. Rev. D **79** (2009) 083528 [[arXiv:0811.0399](#)].
- [45] J. Kopp, V. Niro, T. Schwetz and J. Zupan, Phys. Rev. D **80**, 083502 (2009) [[arXiv:0907.3159](#)].
- [46] P. Agrawal, S. Blanchet, Z. Chacko and C. Kilic, [arXiv:1109.3516](#).
- [47] M. Pospelov and T. ter Veldhuis, Phys. Lett. B **480**, 181 (2000) [[hep-ph/0003010](#)].
- [48] K. Sigurdson, M. Doran, A. Kurylov, R. R. Caldwell and M. Kamionkowski, Phys. Rev. D **70**, 083501 (2004) [Erratum-ibid. D **73**, 089903 (2006)] [[astro-ph/0406355](#)].
- [49] E. Masso, S. Mohanty and S. Rao, Phys. Rev. D **80**, 036009 (2009) [[arXiv:0906.1979](#)].
- [50] S. Chang, N. Weiner and I. Yavin, Phys. Rev. D **82**, 125011 (2010) [[arXiv:1007.4200](#)].
- [51] V. Barger, W. Y. Keung and D. Marfatia, Phys. Lett. B **696**, 74 (2011) [[arXiv:1007.4345](#)].
- [52] W. S. Cho, J. H. Huh, I. W. Kim, J. E. Kim and B. Kyae, Phys. Lett. B **687**, 6 (2010) [Erratum-ibid. B **694**, 496 (2011)] [[arXiv:1001.0579](#)].
- [53] A. L. Fitzpatrick and K. M. Zurek, Phys. Rev. D **82**, 075004 (2010) [[arXiv:1007.5325](#)].
- [54] T. Banks, J. -F. Fortin and S. Thomas, [arXiv:1007.5515](#) [hep-ph].
- [55] K. Abe *et al.* [T2K Collaboration], Phys. Rev. Lett. **107** (2011) 041801 [[arXiv:1106.2822](#)].

- [56] T. Schwetz, M. Tortola and J. W. F. Valle, New J. Phys. **13** (2011) 109401 [[arXiv:1108.1376](#)].
- [57] Y. Abe *et al.* [DoubleChooz Collaboration], [arXiv:1112.6353](#) [hep-ex].
- [58] K. Hayasaka *et al.* [Belle Collaboration], Phys. Lett. B **666**, 16 (2008) [[arXiv:0705.0650](#)].
- [59] J. Adam *et al.* [MEG collaboration], [arXiv:1107.5547](#) [hep-ex].
- [60] O. Adriani *et al.* [PAMELA Collaboration], Nature **458**, 607 (2009) [[arXiv:0810.4995](#)].
- [61] M. Ackermann *et al.* [Fermi LAT Collaboration], Phys. Rev. D **82**, 092004 (2010) [[arXiv:1008.3999](#)].
- [62] M. Ackermann *et al.* [The Fermi LAT Collaboration], [arXiv:1109.0521](#) [astro-ph.HE].
- [63] J. Hisano, S. Matsumoto, M. M. Nojiri and O. Saito, Phys. Rev. D **71**, 063528 (2005) [[hep-ph/0412403](#)].
- [64] D. Feldman, Z. Liu and P. Nath, Phys. Rev. D **79**, 063509 (2009) [[arXiv:0810.5762](#)].
- [65] M. Ibe, H. Murayama and T. T. Yanagida, Phys. Rev. D **79**, 095009 (2009) [[arXiv:0812.0072](#)].
- [66] K. Griest and D. Seckel, Phys. Rev. D **43**, 3191 (1991).
- [67] K. Jedamzik, Phys. Rev. D **74**, 103509 (2006) [[hep-ph/0604251](#)].
- [68] D. Tucker-Smith and N. Weiner, Phys. Rev. D **64**, 043502 (2001) [[hep-ph/0101138](#)].
- [69] D. Tucker-Smith and N. Weiner, Phys. Rev. D **72**, 063509 (2005) [[hep-ph/0402065](#)].
- [70] S. Patra and S. Rao, [arXiv:1112.3454](#).
- [71] M. T. Ressell and D. J. Dean, Phys. Rev. C **56**, 535 (1997) [[hep-ph/9702290](#)].
- [72] V. A. Bednyakov and F. Simkovic, Phys. Part. Nucl. **37**, S106 (2006) [[hep-ph/0608097](#)].
- [73] J. R. Ellis and R. A. Flores, Phys. Lett. B **263**, 259 (1991).
- [74] C. McCabe, Phys. Rev. D **82**, 023530 (2010) [[arXiv:1005.0579](#)].
- [75] B. Feldstein, P. W. Graham and S. Rajendran, Phys. Rev. D **82**, 075019 (2010) [[arXiv:1008.1988](#)].